


**Coulomb sum rule in the quasielastic region using various nuclear models**

K. S. Kim\*

*School of Liberal Arts and Science, Korea Aerospace University, Goyang, 10540, Korea*

Soonchul Choi

*Center for Exotic Nuclear Studies, Institute for Basic Science (IBS), Daejeon 34126, Korea*Myung-Ki Cheoun *Department of Physics and Origin of Matter and Evolution of Galaxy (OMEG) Institute, Soongsil University, Seoul 06978, Korea*

Hungchong Kim

*Center for Extreme Nuclear Matters, Korea University, seoul 02841, Korea*

(Received 12 August 2021; revised 24 October 2021; accepted 20 December 2021; published 9 February 2022)

We calculate the Coulomb sum rule of inclusive ( $e, e'$ ) reactions from  $^{12}\text{C}$ ,  $^{40}\text{Ca}$ ,  $^{56}\text{Fe}$ , and  $^{208}\text{Pb}$  in the quasielastic region using various relativistic single-particle models, which include the relativistic Hartree, the nonlinear sigma, the quark-meson-coupling, and the chiral quark-meson-coupling models. We investigate the cross sections calculated in these nuclear models by comparing them with Bates, Saclay, and SLAC data for three-momentum transfer  $q$  ranging from 300 to 500 MeV/ $c$ . We find that the extracted longitudinal structure functions are not so sensitive to the nuclear model but the transverse structure functions strongly depend on the model. We report that, for three-momentum transfer  $q > 400$  MeV/ $c$ , the values of the Coulomb sum rule from various nuclear models except the Hartree model are greater than 1.

DOI: [10.1103/PhysRevC.105.024606](https://doi.org/10.1103/PhysRevC.105.024606)**I. INTRODUCTION**

Medium and high energy electron scattering has long been acknowledged as a useful tool to study not only nuclear structure and properties but also nucleon properties inside nuclei in the quasielastic (QE) region where individual nucleons have Fermi motion. In this paper we concentrate on the inclusive ( $e, e'$ ) reaction that probes all of the nucleons in the nucleus and is not so sensitive to individual orbits and energy levels. There is considerable experimental and theoretical interest in extracting longitudinal and transverse structure functions as a function of energy transfer at fixed three-momentum transfer because the two structure functions represent the electric and magnetic responses of the target nucleus, respectively.

The Coulomb sum rule (CSR) was proposed as a tool to study short-range correlations between nucleons. The correlations occur strongly at large energy transfer, and at large momentum transfer these go to zero in the CSR. The Fermi gas model, which is a simple nuclear model, furnishes a rough description of the inclusive ( $e, e'$ ) cross sections in the impulse approximation but fails in describing the structure functions. In particular, there appears to be a large suppression (about 40–50%) of the longitudinal structure function, corresponding to missing strength in the CSR [1]. In early works [2,3], this suppression has been interpreted as a nuclear medium effect

which increases the charge radius and quenches the anomalous moments.

There were many attempts [1,4–8] to explain the missing strength of the longitudinal structure function by improving the nuclear bound states, modifying the nucleon form factors in the nuclear medium, including final state interactions, relativistic dynamics effects, and so on. In Ref. [9], the CSR was analyzed based on scaling and superscaling methods for  $^{12}\text{C}$ ,  $^{40}\text{Ca}$ , and  $^{56}\text{Fe}$  by using various descriptions of the final state interaction in the relativistic impulse approximation, and then the value of the CSR saturates to 0.9 at three-momentum transfer  $q \leq 500$  MeV/ $c$ . Using quantum chromodynamics, the CSR was calculated for momentum transfer  $q \gtrsim 500$  GeV/ $c$  and it was found to be suppressed significantly [10]. The cross sections were calculated in the superscaling (SuSAv2) model that includes two-particle two-hole meson-exchange currents to describe the dip region. These show good agreement with experimental data over the full energy spectrum [11]. The roles of the real part for various relativistic optical potentials were investigated by calculating QE cross sections with the SuSAv2 model for three-momentum transfer  $50 < q < 1500$  MeV/ $c$  [12].

On the other hand, on the experimental side, there have been two measurements showing suppression of the CSR: One is that the suppression was about 30% for three-momentum transfer  $300 \leq q \leq 450$  MeV/ $c$  on  $^{40}\text{Ca}$ , measured by Bates [5,6]. The other one is that the suppressions appeared to be about 50% in effective three-momentum transfer values from

\*kyungsik@kau.ac.kr

350 to 550 MeV/ $c$  on  $^{208}\text{Pb}$  at Saclay [7]. While the suppression of the CSR depends on the nucleus [13], Jourdan [14] had analyzed the experimental data for  $^{12}\text{C}$ ,  $^{40}\text{Ca}$ , and  $^{56}\text{Fe}$  and found that there is no  $A$ -dependent quenching for the Coulomb sum and the suppression of the longitudinal structure function is about 30%, similar to the results of Bates [5,6]. Furthermore, Morgenstern and Mezzani [15] reanalyzed the experimental data of  $^{40}\text{Ca}$ ,  $^{48}\text{Ca}$ ,  $^{56}\text{Fe}$ ,  $^{197}\text{Au}$ ,  $^{208}\text{Pb}$ , and  $^{238}\text{U}$  at the effective three-momentum transfer 500 MeV/ $c$  and they found that the longitudinal structure function is suppressed by about 40% at that value. However, Kim and *et al.* [16] claimed that the suppression of the CSR was not found to be near 50% as obtained from Saclay group [7,15], by using the relativistic nuclear model based on the  $\sigma$ - $\omega$  model [17].

Recently, the Mainz group [18] calculated the CSR for  $^4\text{He}$  and  $^{16}\text{O}$  from coupled-cluster theory by using chiral effective field theory with various potentials up to three-momentum transfer  $q = 500$  MeV/ $c$ . At JLab [19], the experiment of the CSR was performed with energies from 0.4 to 4 GeV for  $^4\text{He}$ ,  $^{12}\text{C}$ ,  $^{56}\text{Fe}$ , and  $^{208}\text{Pb}$  nuclei at four different scattering angles,  $15^\circ$ ,  $60^\circ$ ,  $90^\circ$ , and  $120^\circ$ . In the range  $0.55 \leq q \leq 1.0$  GeV/ $c$ , the CSR was measured in testing the Coulomb corrections.

There are two issues in comparing theoretical ( $e$ ,  $e'$ ) results with experimental data. One is the treatment of the incident and outgoing electrons for the Coulomb distortion from target nucleus. In the early 1990s, the Ohio group [20] calculated the ( $e$ ,  $e'$ ) reaction by using partial wave expansion of the electron wave functions. Although this method handles exactly the Coulomb distortion of the electrons, the calculated cross section cannot be separated into various response functions and the computational time increases rapidly with higher electron energies. To avoid these difficulties, Kim and Wright [21] developed an approximate Coulomb distortion based on the works of Knoll [22] and of Lenz and Rosenfelder [23].

The second issue is how to describe the target nucleus. There are various nuclear models constructed in either a nonrelativistic or relativistic manner. The most simple and economical one is the relativistic Hartree single-particle model (quantum hadrodynamics, QHD) [17,24] used in the mean field level. This relativistic single-particle model has been widely used for studying nuclear structure, nuclear reactions, and so on. The nonlinear (NL) sigma model is also one of the relativistic single-particle models but it includes nonlinear scalar self-coupling among the  $\sigma$  mesons [25]. The quark-meson-coupling (QMC) model [26] is somewhat different in that the nucleon in nuclear medium is described to be a nonoverlapping MIT bag bound by the self-consistent exchange of  $\sigma$ ,  $\omega$ , and  $\rho$  mesons, and the chiral QMC (CQMC) model [27] improves the QMC model by including the effect of gluon exchange as well as the pion cloud effect using volume coupling of the cloudy bag model. Recently, we calculated the exclusive ( $e$ ,  $e'p$ ) reactions [28] in the QE region by using four different nuclear models, QHD, NL, QMC, and CQMC, and reported that the dependence on these nuclear models is not so evident.

On the other hand, in our previous works [29–31], the QHD model has been used for properly explaining the inclusive QE electron scattering data, and also successfully applied to many neutrino QE scattering data accumulated from MiniBooNE

and Minerva. In particular, these days both structure functions are now intensively discussed in the neutrino scattering off finite nuclei in the QE region because the response functions play important roles in understanding the cross sections with an additional structure function, the transverse interference structure function, coming from the neutrino helicity [29]. For example, the asymmetry data from neutrino ( $\nu$ ) and antineutrino ( $\bar{\nu}$ ) scattering for neutral-current (NC) reactions off  $^{12}\text{C}$  [30] and the double differential cross section for charged-current  $\bar{\nu}_\mu$ - $^{12}\text{C}$  scattering are well explained within the QHD model with the standard axial mass in the axial form factor including the strangeness contribution to the NC scattering [31]. The authors of Ref. [32] studied the relationship between elastic electron scattering and neutrino scattering for even-even nuclei by using the Hartree-Fock mean field. The longitudinal, transverse, and transverse-interference structure functions were extracted by using the Rosenbluth separation with the QHD model and then the axial and pseudoscalar terms played an important role in the QE neutrino-nucleus scattering [33]. The structure functions were compared from QE electron and neutrino scattering within an asymmetric and relativistic Fermi gas model, which takes into account the difference between proton and neutron densities in asymmetric ( $N > Z$ ) nuclei [34].

In this work, we investigate the CSR by comparing with Bates and Saclay data for three-momentum transfer ranging from 300 to 500 MeV/ $c$  in the QE region. For the Coulomb distortion of the electrons, we use the same approximation exploited by the Ohio group [35]. To avoid the violation of current conservation and gauge invariance we use the same potentials for the bound state and continuum state of nucleons. In Sec. II the formalism of the ( $e$ ,  $e'$ ) reaction in QE region is briefly discussed and in Sec. III we present the cross sections and the CSR. Finally, a summary and conclusions are given in Sec. IV.

## II. FORMALISM

In the plane wave Born approximation (PWBA) in which the electrons are described as Dirac plane waves, the cross section for the inclusive ( $e$ ,  $e'$ ) reaction can be written as

$$\frac{d^2\sigma}{d\omega d\Omega_e} = \sigma_M \left[ \frac{Q^4}{q^4} S_L(q, \omega) + \left( \tan^2 \frac{\theta_e}{2} + \frac{Q^2}{2q^2} \right) S_T(q, \omega) \right], \quad (1)$$

where  $Q^2 = \mathbf{q}^2 - \omega^2 = -q_\mu^2$  is the four-momentum transfer squared,  $\sigma_M$  is the Mott cross section given by  $\sigma_M = \left( \frac{\alpha}{2E_i} \right)^2 \cos^2 \left( \frac{\theta_e}{2} \right) / \sin^4 \left( \frac{\theta_e}{2} \right)$ , and  $S_L$  and  $S_T$  are the longitudinal and transverse structure functions which depend only on the three-momentum transfer  $q$  and the energy transfer  $\omega$ . By keeping the three-momentum and energy transfers fixed while varying the electron incident energy  $E_i$  and scattering angle  $\theta_e$ , it is possible to extract the two structure functions with two measurements. The longitudinal and transverse structure functions in Eq. (1) are squares of the Fourier transform of the components of the nuclear transition current density integrated over outgoing nucleon angles,  $\Omega_p$ . Explicitly, the

structure functions for a given bound state with angular momentum  $j_b$  are given by

$$S_L(q, \omega) = \sum_{\mu_b s_p} \frac{\rho_p}{2(2j_b + 1)} \int |N_0|^2 d\Omega_p, \quad (2)$$

$$S_T(q, \omega) = \sum_{\mu_b s_p} \frac{\rho_p}{2(2j_b + 1)} \int (|N_x|^2 + |N_y|^2) d\Omega_p \quad (3)$$

with the outgoing nucleon density of states  $\rho_p = \frac{pE_p}{(2\pi)^3}$ . The  $\hat{z}$  axis is taken to be along the momentum transfer  $\mathbf{q}$  and the  $z$  components of the angular momentum of the bound and continuum state nucleons are denoted as  $\mu_b$  and  $s_p$ , respectively. The Fourier transform of the nuclear current  $J^\mu(\mathbf{r})$  is simply given by

$$N^\mu = \int J^\mu(\mathbf{r}) e^{i\mathbf{q}\cdot\mathbf{r}} d^3r, \quad (4)$$

where  $J^\mu(\mathbf{r})$  denotes the nucleon transition current. The continuity equation could be used to eliminate the  $z$  component ( $N_z$ ) via the equation  $N_z = -\frac{\omega}{q} N_0$  if the current is conserved. The nucleon transition current in the relativistic single particle model is given by

$$J^\mu(\mathbf{r}) = e\bar{\psi}_p(\mathbf{r})\hat{\mathbf{J}}^\mu\psi_b(\mathbf{r}), \quad (5)$$

where  $\hat{\mathbf{J}}^\mu$  is a free nucleon current operator, and  $\psi_p$  and  $\psi_b$  are the wave functions of the knocked-out nucleon and the bound state, respectively. For a free nucleon, the operator comprises the Dirac contribution and the contribution of an anomalous magnetic moment  $\mu_T$  given by  $\hat{\mathbf{J}}^\mu = F_1(q_\mu^2)\gamma^\mu + F_2(q_\mu^2)\frac{i\mu_T}{2M_N}\sigma^{\mu\nu}q_\nu$ , where  $M_N$  is the mass of a nucleon. The form factors  $F_1$  and  $F_2$  are related to the electric and magnetic Sachs form factors given by  $G_E = F_1 + \frac{\mu_T Q^2}{4M_N^2} F_2$  and  $G_M = F_1 + \mu_T F_2$ , which are assumed to take the following standard form:

$$G_E = \frac{1}{(1 + \frac{Q^2}{\Lambda^2})^2} = \frac{G_M}{(\mu_T + 1)}, \quad (6)$$

where the standard value for  $\Lambda^2$  is  $0.71 (\text{GeV}/c)^2$ .

From the measured cross section in Eq. (1), the total structure function can be defined as

$$S_{tot}(q, \omega, \theta_e) = \left( \frac{\epsilon(\theta_e)}{\sigma_M} \right) \left( \frac{q^4}{Q^4} \right) \frac{d^2\sigma}{d\omega d\Omega_e}, \quad (7)$$

where the  $\epsilon(\theta_e)$  is the virtual photon polarization given by  $\epsilon(\theta_e) = [1 + (\frac{2q^2}{Q^2}) \tan^2(\theta_e/2)]^{-1}$ . Therefore, the total structure function in Eq. (7) becomes

$$S_{tot}(q, \omega, \theta_e) = \epsilon(\theta_e) S_L(q, \omega) + \left( \frac{q^2}{2Q^2} \right) S_T(q, \omega). \quad (8)$$

$S_{tot}$  is described as a straight line in terms of the independent variable  $\epsilon(\theta_e)$  with slope  $S_L(q, \omega)$  and intercept proportional to  $S_T(q, \omega)$  by keeping the momentum transfer  $q$  and the energy transfer  $\omega$  fixed. This is called Rosenbluth separation.

The CSR is defined as the integration of the longitudinal structure function in Eq. (8) by de Forest [36],

$$C(q) = \frac{1}{Z} \int_{\omega_{\min}}^{\infty} \frac{S_L(q, \omega)}{\tilde{G}_E^2(Q^2)} d\omega, \quad (9)$$

with the modified electric form factor given by

$$\tilde{G}_E^2(Q^2) = \left[ G_{E_p}^2(Q^2) + \frac{N}{Z} G_{E_n}^2(Q^2) \right] \frac{(1 + \tau)}{(1 + 2\tau)}, \quad (10)$$

where  $Z$  and  $N$  denote numbers of protons and neutrons of the target, respectively.  $G_{E_p}$  and  $G_{E_n}$  represent the Sachs electric form factors for the protons and neutrons, respectively. The last factor corresponds to the relativistic correction factor, in which  $\tau$  is given by  $\tau = Q^2/4M_N^2$ . The lower limit  $\omega_{\min}$  in the integration includes all inelastic contributions but excludes the elastic process. For  $\omega > q$ , one has to neglect the longitudinal structure function on integrating over the infinite range of the  $\omega$  because it cannot be accessible with the QE electron scattering.

Neglecting the small contribution from the neutron charge form factor, the integral over the longitudinal structure function can be regarded as the number of protons times the square of the proton charge form factor  $G_{E_p}^2$ . When the nuclear elastic charge form factor falls rapidly with increasing three-momentum transfer  $q$ , the CSR becomes  $C(q) = 1$  in the limit  $q \rightarrow \infty$ .

In addition, at low  $q$  below twice the Fermi momentum ( $k_F$ ), the longitudinal structure function is affected by Pauli blocking [37]. This low momentum transfer is not sufficient to send some initial nucleons to unoccupied states above the Fermi level. Therefore, both longitudinal and transverse structure functions are moved to the lower  $\omega$  of the peak, and the  $\omega$  dependence is almost linear in this blocked region. For  $q > 2k_F$  the Pauli blocking between nucleons does not occur for all nucleons momenta. The  $\omega$  dependence is roughly parabolic, with the width of the peak being proportional to  $k_F$ , and the position of the peak is shifted toward the higher  $\omega$ . For example, at large  $q$ , typically above  $0.8 \text{ GeV}/c$ , the transverse structure function dominates the cross section and the inelastic processes like the  $\Delta$  contribution increase, so that an exact measurement of the longitudinal structure function is very difficult.

### III. RESULTS

With four different nuclear models, we calculate the inclusive ( $e, e'$ ) cross sections and also study the CSR by comparing with Bates and Saclay data in the  $q$  range from 300 to 500 MeV/ $c$  in the QE region. To include the final state interaction, the wave functions of the final nucleons are generated by using the same potential as the bound state of nucleons. This method is taken to avoid the violation of current conservation and to guarantee the gauge invariance. Notice that we use the same lepton part and the same current operator of the hadron to compare with these different nuclear models. In all calculations, the four-momentum transfer squared  $Q^2$  is in the range 0.1–0.3 (GeV/ $c$ )<sup>2</sup>. The scattering angles for <sup>40</sup>Ca are used 45.5°, 90°, 140° in Ref. [6], and those for <sup>208</sup>Pb are used 35°, 60°, 90°, and 143° in Ref. [7].

Figure 1 shows the inclusive QE cross sections on <sup>40</sup>Ca obtained from four different nuclear models. The solid curves (red) are the results for the relativistic Hartree model (labeled QHD), the dotted lines (blue) are for the non-linear sigma model (labeled NL), the dash-dotted curves (sky blue) are

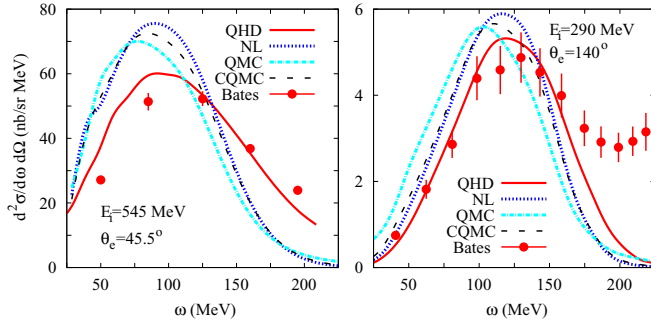


FIG. 1. The cross sections on  $^{40}\text{Ca}$  from four different nuclear models. The solid curves (red) are the results for the Hartree model, the dotted lines (blue) are for the nonlinear sigma model, the dash-dotted curves (sky blue) are for the QMC model, and the dashed curves are for the chiral QMC model. The experimental data were measured by Bates [5,6].

for the QMC model (labeled QMC), and the dashed curves (black) are for the chiral QMC model (labeled CQMC). The kinematics of the left (right) panel are the incident electron energies  $E_i = 545$  MeV (290 MeV) and the scattering angles  $\theta_e = 45.5^\circ$  ( $140^\circ$ ). The experimental data were measured by Bates [5,6]. The cross sections from the other models except the QHD overestimate the experimental data and the positions of the peak shift toward lower energy transfer. The largest difference between the red and the blue curves at forward angle is about 20% and at backward angle it amounts to about 30%. Note that the theoretical cross sections at large energy transfer region do not describe the data at all because the inelastic processes like pion production or delta resonance are excluded.

In Fig. 2, the inclusive QE cross sections on  $^{208}\text{Pb}$  are calculated from four different nuclear models. The explanations for the curves are the same as those in Fig. 1. The kinematics of the left (right) panel are the incident electron energies  $E_i = 485$  MeV (262 MeV) and the scattering angles  $\theta_e = 60^\circ$  ( $143^\circ$ ). The experimental data were measured from Saclay [7]. The cross sections from the other models except QHD overestimate the experimental data and the positions of the peak shift toward lower energy transfer like the previous results for  $^{40}\text{Ca}$  in Fig. 1. The magnitude of the cross section

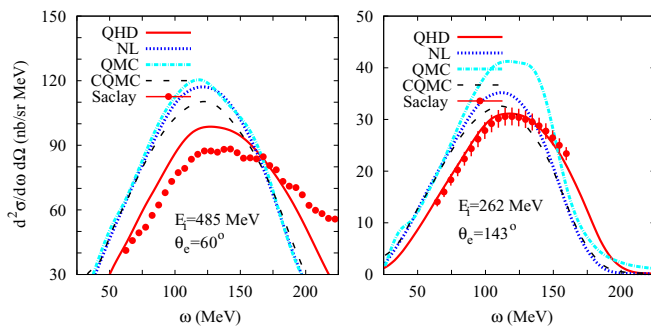


FIG. 2. The cross sections on  $^{208}\text{Pb}$  from four different nuclear models. The explanations for the curves are the same as those in Fig. 1. The experimental data were measured by Saclay [7].

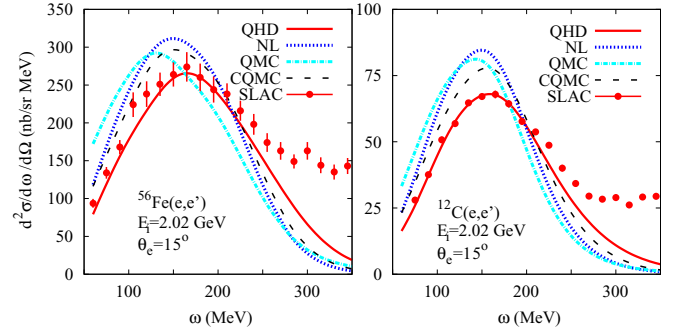


FIG. 3. The inclusive QE cross sections on  $^{56}\text{Fe}$  and  $^{12}\text{C}$  are presented from four different nuclear models. The explanations for the curves are the same as those in Fig. 1. The experimental data were measured by SLAC [8].

for the QMC model is largest on  $^{208}\text{Pb}$  around the peak while the magnitude of the cross section for NL model is largest around the peak on  $^{40}\text{Ca}$ . The largest difference between the red and the sky blue curves at forward and backward angles is similar to the previous one in Fig. 1.

On the other hand, there are other experimental data measured from SLAC [8] and JLab [38] for high electron energies. In our previous works [39], our model could not describe the data for such high energies except for a few cases of 2 GeV and very forward angle because the nuclear model basically adopts the partial wave expansion, although the lepton part is the approximation without the expansion.

In Fig. 3, the inclusive QE cross sections on  $^{56}\text{Fe}$  and  $^{12}\text{C}$  are presented from four different nuclear models. The explanations for the curves are the same as those in Fig. 1. The kinematics of both panels are the incident electron energies  $E_i = 2.02$  GeV and the scattering angles  $\theta_e = 15^\circ$ . The experimental data were measured from SLAC [8]. The cross sections from the other models except QHD overestimate the experimental data, and the positions of the peak shift toward lower energy transfer like the previous results in Figs. 1 and 2. In this case, the magnitude of the cross section for the NL model is largest around the peak as in the case of  $^{40}\text{Ca}$ . The largest difference between the red and the blue curves is similar to the previous results in Figs. 1 and 2. From these results, we do not find any regular pattern. In particular, the calculations of the QHD model describe the SLAC experimental very well.

In our previous paper [28], the exclusive  $(e, e'p)$  cross sections were calculated at the  $2s_{1/2}$  and  $1d_{3/2}$  shells of  $^{40}\text{Ca}$  for both parallel and perpendicular kinematics with four different relativistic single-particle nuclear models: QHD, nonlinear sigma, QMC, and CQMC, as this work. According to this paper, it is not easy to distinguish a difference between the models although they include effectively the influence of nucleon structure in nuclear medium. However, in the  $(e, e')$  reaction, it is necessary to sum over all nucleons inside the target nucleus to calculate the cross section in Eqs. (2) and (3). For this reason, the difference between the relativistic nuclear models is accumulated to about 20%–30% even if the difference among the models is small.

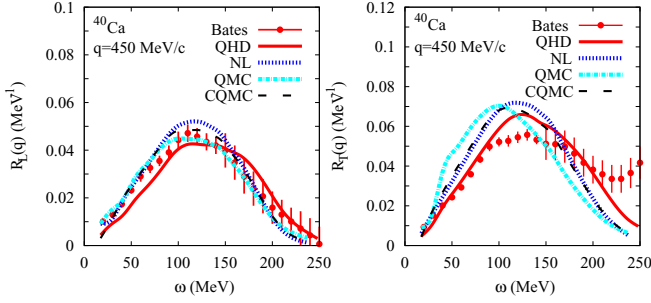


FIG. 4. The extracted longitudinal and transverse structure functions at  $q = 450$  MeV/ $c$  off  $^{40}\text{Ca}$  from four different nuclear models. The experimental data were measured by Bates [5,6].

In Figs. 4 and 5, the extracted longitudinal and transverse structure functions in Eq. (8) are presented for  $^{40}\text{Ca}$  and  $^{208}\text{Pb}$  at three-momentum transfer  $q = 450$  MeV/ $c$ . Like the cross sections in Fig. 1, the magnitude of the longitudinal and transverse structure functions for NL model is largest around the peak on  $^{40}\text{Ca}$  and the positions of the peak shift toward lower energy transfer. In Fig. 4, the longitudinal structure functions from the models describe the Bates data relatively well but the all transverse structure functions overestimate the data around the peak.

In Fig. 5, the shapes and positions extracted from longitudinal structure functions for  $^{208}\text{Pb}$  are different from those in the cross sections in Fig. 2, though those of the transverse structure functions are similar to the cross section. The reason is that the magnitude of the longitudinal functions is about 55% compared to that of the transverse functions. It means that the contribution of the longitudinal functions turns out to be about 30%. Furthermore, the theoretical longitudinal functions do not describe the Saclay data at all, even including the QMC model describe the data well.

To calculate the CSR, it is necessary to determine the lower and upper limits of the integration in Eq. (9). We choose  $\omega_{\min} = 10$  MeV to exclude the elastic process in all calculations, but the exact values of  $\omega_{\min}$  in the Bates [6] and Saclay [7] papers were not shown. In the case of the upper limit  $\omega_{\max}$ , we use different values from 190 to 250 MeV like the Bates and Saclay papers. In particular,

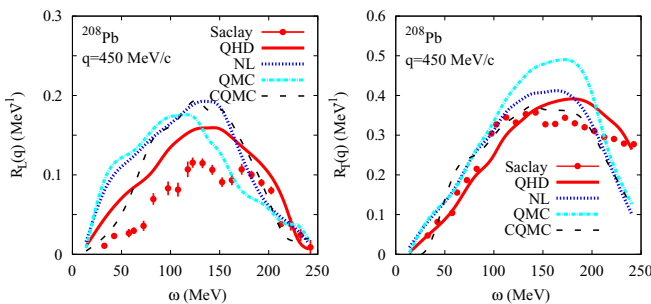


FIG. 5. The extracted longitudinal and transverse structure functions at  $q = 450$  MeV/ $c$  off  $^{208}\text{Pb}$  from four different nuclear models. The experimental data were measured by Saclay [7].

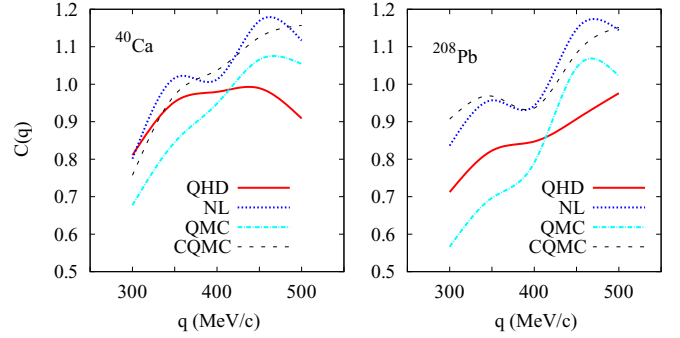


FIG. 6. The CSR from four different nuclear models for  $^{40}\text{Ca}$  and  $^{208}\text{Pb}$ .

according to Ref. [1], the value of  $\omega_{\max}$  is the experimental limit beyond which data are unreliable because of electron-pair contamination and detector inefficiency. The values of  $\omega_{\max}$  were chosen from 175 to 310 MeV in the range of three-momentum transfer  $330 < q < 550$  MeV/ $c$  for  $^{40}\text{Ca}$  and  $^{48}\text{Ca}$ .

In Fig. 6, we present the CSR  $C(q)$  values using these upper limits within four different nuclear models. While the shapes are similar to each other in the cross sections and the structure functions, the shapes of  $C(q)$  are not similar at all; in particular, the NL model has minimum value around  $q = 400$  MeV/ $c$ . In comparison with Bates experimental data in Fig. 19 of Ref. [6], the QHD model has similar tendency but other models have totally different shape. The theoretical values of  $C(q)$  for  $^{208}\text{Pb}$  show different tendency compared to Saclay data in Fig. 21 of Ref. [7]. The values of  $C(q)$  obtained from the three models except the QHD model are greater than 1 above the  $q = 400$  MeV/ $c$  region, implying violation of the CSR.

#### IV. SUMMARY AND CONCLUSION

In the present work, we calculate the inclusive ( $e, e'$ ) cross sections and extract the longitudinal and transverse structure functions by using the Rosenbluth separation with four different nuclear models, which are the relativistic Hartree model (QHD), the nonlinear sigma model, the QMC model, and the CQMC model. Furthermore, the cross sections are compared with SLAC experimental data for high electron energy. Except for the QHD model which has been successfully applied to neutrino-nucleus scattering, the magnitudes of the theoretical cross sections overestimate the experimental data and the positions of the peak shift toward lower energy loss. The extracted longitudinal structure functions of  $^{40}\text{Ca}$  describe the Bates data relatively well but for  $^{208}\text{Pb}$  overestimate the Saclay data, and the transverse structure functions of  $^{40}\text{Ca}$  overestimate the Bates data but for  $^{208}\text{Pb}$  describe the Saclay data except in the QMC model. Finally, the only calculated CSR from the QHD on  $^{40}\text{Ca}$  has a pattern similar to the experimental data; in particular, the CSR from the NL model has a minimum around  $q = 400$  MeV/ $c$ . In the  $q > 400$  MeV/ $c$  region, the values of the CSR are greater

than ones obtained from other nuclear models except the QHD model.

In conclusion, it will be necessary to provide a good description with experimental data, such as Bates, Saclay, and SLAC data, by improving the present nuclear models, for example, including the pairing correlation effect beyond the relativistic mean field theory. But it should be remembered that the present calculation exploited the same form factors for each model because we want to compare the differences due to the wave functions among the nuclear models. More deliberate form factors, such as a form factor including the nuclear matter effect [10], may help to properly interpret the

CSR quenching with additional effects from collective motions, as in the random phase approximation (RPA).

#### ACKNOWLEDGMENTS

The work of K.S.K. and H.K. was supported by the National Research Foundation of Korea (Grants No. NRF-2018R1A5A1025563 and No. NRF-2018R1A2B6002432), M.-K.C. was supported by the National Research Foundation of Korea (Grants No. NRF-2020R1A2C3006177 and No. NRF-2021R1A6A1A03043957), and S.C. was supported by the Institute for Basic Science (IBS-R031-D1).

- 
- [1] Z. E. Meziani *et al.*, *Nucl. Phys. A* **446**, 113 (1985); *Phys. Rev. Lett.* **52**, 2130 (1984); **54**, 1233 (1985).
- [2] J. V. Noble, *Phys. Rev. Lett.* **46**, 412 (1981).
- [3] L. S. Celenza, A. Harindranath, and C. M. Shakin, *Phys. Rev. C* **33**, 1012 (1986).
- [4] P. Barreau *et al.*, *Nucl. Phys. A* **402**, 515 (1983).
- [5] M. Deady, C. F. Williamson, J. Wong, P. D. Zimmerman, C. Blatchley, J. M. Finn, J. LeRose, P. Sioshansi, R. Altemus, J. S. McCarthy, and R. R. Whitney, *Phys. Rev. C* **28**, 631 (1983); M. Deady, C. F. Williamson, P. D. Zimmerman, R. Altemus, and R. R. Whitney, *ibid.* **33**, 1897 (1986); C. C. Blatchley, J. J. LeRose, O. E. Pruet, P. D. Zimmerman, C. F. Williamson, and M. Deady, *ibid.* **34**, 1243 (1986).
- [6] C. F. Williamson, T. C. Yates, W. M. Schmitt, M. Osborn, M. Deady, P. D. Zimmerman, C. C. Blatchley, K. K. Seth, M. Sarmiento, B. Parker, Y. Jin, L. E. Wright, and D. S. Onley, *Phys. Rev. C* **56**, 3152 (1997); T. C. Yates *et al.*, *Phys. Lett. B* **312**, 382 (1993).
- [7] A. Zghiche *et al.*, *Nucl. Phys. A* **572**, 513 (1994).
- [8] D. B. Day, J. S. McCarthy, Z. E. Meziani, R. Minehart, R. Sealock, S. T. Thornton, J. Jourdan, I. Sick, B. W. Filippone, R. D. McKeown, R. G. Milner, D. H. Potterveld, and Z. Szalata, *Phys. Rev. Lett.* **59**, 427 (1987); D. B. Day *et al.*, *Phys. Rev. C* **48**, 1849 (1993).
- [9] J. A. Caballero, M. C. Martinez, J. L. Herraiz, and J. M. Udias, *Phys. Lett. B* **688**, 250 (2010).
- [10] Ian C. Cloet, W. Bentz, and Anthony W. Thomas, *Phys. Rev. Lett.* **116**, 032701 (2016).
- [11] M. B. Barbaro, J. A. Caballero, A. De Pace, T. W. Donnelly, R. Gonzalez-Jimenez, and G. D. Megias, *Phys. Rev. C* **99**, 042501(R) (2019).
- [12] R. Gonzalez-Jimenez, M. B. Barbaro, J. A. Caballero, T. W. Donnelly, N. Jachowicz, G. D. Megias, K. Niewczas, A. Nikolakopoulos, and J. M. Udias, *Phys. Rev. C* **101**, 015503 (2020).
- [13] M. Traini, *Phys. Lett. B* **213**, 1 (1988).
- [14] J. Jourdan, *Nucl. Phys. A* **603**, 117 (1996).
- [15] J. Morgenstern and Z. E. Meziani, *Phys. Lett. B* **515**, 269 (2001).
- [16] K. S. Kim, B. G. Yu, and M. K. Cheoun, *Phys. Rev. C* **74**, 067601 (2006).
- [17] C. J. Horowitz and B. D. Serot, *Nucl. Phys. A* **368**, 503 (1981).
- [18] J. E. Sobczyk, B. Acharya, S. Bacca, and G. Hagen, *Phys. Rev. C* **102**, 064312 (2020).
- [19] M. Paolone, in *International Workshop on Physics with Positrons at Jefferson Lab*, 12–15 September 2017, Newport News, VA, AIP Conf. Proc. No. 1970 (AIP, New York, 2018), p. 020010.
- [20] Y. Jin, D. S. Onley, and L. E. Wright, *Phys. Rev. C* **45**, 1311 (1992); **45**, 1333 (1992).
- [21] K. S. Kim, L. E. Wright, Y. Jin, and D. W. Kosik, *Phys. Rev. C* **54**, 2515 (1996); K. S. Kim and L. E. Wright, *ibid.* **56**, 302 (1997).
- [22] J. Knoll, *Nucl. Phys. A* **201**, 289 (1973); **223**, 462 (1974).
- [23] F. Lenz and R. Rosenfelder, *Nucl. Phys. A* **176**, 513 (1971).
- [24] J. D. Walecka, *Ann. Phys. (NY)* **83**, 491 (1974).
- [25] P. Ring, *Prog. Part. Nucl. Phys.* **37**, 193 (1996).
- [26] K. Saito, K. Tsushima, and A. W. Thomas, *Nucl. Phys. A* **609**, 339 (1996); *Phys. Rev. C* **55**, 2637 (1997).
- [27] S. Nagi, T. Miyatsu, K. Saito, and K. Tsushima, *Phys. Lett. B* **666**, 239 (2008).
- [28] S. Choi, T. Miyatsu, Y. Kwon, K. Kim, M.-K. Cheoun, and K. Saito, *Phys. Rev. C* **104**, 014322 (2021).
- [29] K. S. Kim, M.-K. Cheoun, and B. G. Yu, *Phys. Rev. C* **77**, 054604 (2008); K. S. Kim, B. G. Yu, M. K. Cheoun, T. K. Choi, and M. T. Chung, *J. Phys. G: Nucl. Part. Phys.* **34**, 2643 (2007).
- [30] K. S. Kim, H. Kim, M.-K. Cheoun, G.-S. Yang, and W. Y. So, *Phys. Rev. C* **92**, 044613 (2015).
- [31] K. S. Kim, K.-S. Choi, M.-K. Cheoun, W. Y. So, and H. Moon, *Phys. Rev. C* **100**, 034604 (2019).
- [32] O. Moreno and T. W. Donnelly, *Phys. Rev. C* **92**, 055504 (2015).
- [33] K. S. Kim, H. Kim, M.-K. Cheoun, and W. Y. So, *Phys. Rev. C* **94**, 064619 (2016).
- [34] M. B. Barbaro, A. De Pace, T. W. Donnelly, J. A. Caballero, G. D. Megias, and J. W. Van Orden, *Phys. Rev. C* **98**, 035501 (2018).
- [35] K. S. Kim, L. E. Wright, and D. A. Resler, *Phys. Rev. C* **64**, 044607 (2001); K. S. Kim and L. E. Wright, *ibid.* **60**, 067604 (1999); **72**, 064607 (2005).
- [36] T. de Forest, *Nucl. Phys. A* **414**, 347 (1984).
- [37] O. Benhar, D. Day, and I. Sick, *Rev. Mod. Phys.* **80**, 189 (2008).
- [38] J. Arrington, C. S. Armstrong, T. Averett, O. K. Baker, L. de Bever, C. W. Bochna, W. Boeglin, B. Bray, R. D. Carlini, G. Collins, C. Cothran, D. Crabb, D. Day, J. A. Dunne, D. Dutta, R. Ent, B. W. Filippone, A. Honegger, E. W. Hughes, J. Jensen *et al.*, *Phys. Rev. Lett.* **82**, 2056 (1999); *Phys. Rev. C* **64**, 014602 (2001).
- [39] K. S. Kim and L. E. Wright, *Phys. Rev. C* **67**, 054604 (2003); K. S. Kim, B. G. Yu, and M. K. Cheoun, *J. Phys. Soc. Jpn.* **75**, 114201 (2006).